PERGAMON

International Journal of Solids and Structures 40 (2003) 4837–4858

INTERNATIONAL JOURNAL OF SOLIDS and STRUCTURES

www.elsevier.com/locate/ijsolstr

Three-dimensional analysis of piezocomposite plates with arbitrary geometry and boundary conditions

H.M. Shodja *, M.T. Kamali

Department of Civil Engineering, Sharif University of Technology, Azadi Ave., P.O. Box 11365-9313, Tehran, Iran

Received 15 August 2002; received in revised form 12 March 2003

Abstract

In this paper, an accurate series solution in conjunction with an energy formulation for the treatment of piezocomposite plates with arbitrary geometry and aspect ratio, under both electrical and mechanical loadings are proposed. A remedy for dealing with nonhomogeneous boundary conditions is also presented. Through introduction of amending polynomials of order p_k for the kth layer, the accuracy and convergence rate are dramatically improved. These polynomials ensure continuity of the generalized displacement fields across the interfaces, while their derivatives can have the required discontinuities up to a desired order. Moreover, depending on the nature of the physical problem under consideration, incorporation of the appropriate functions result in greater convergence rate and precision of the solution.

Keywords: Piezocomposite; Nonhomogeneous boundary conditions; Amending polynomials

1. Introduction

The statical and dynamical applications of piezoelectric materials have a critical role in recent advances and developments of ''smart structures'' and ''smart materials''. Piezoelectrics polarize under applied stresses (direct effect) and deform when subjected to an electric field (converse effect). The desirability of integration of piezoelectric sensors with ''smart structural systems'' is due to their instrumental direct effect for strain measurements. On the other hand, the converse effect of the piezoelectric actuators is implemented for controlling vibrations and elastic deformations of such structures. The early applications were related to control of vibrations of mirrors when subjected to sound vibrations (Forward, 1979). Realizing that local measurements and actuations are not the best means for controlling the continuous behavior of structures, the piezoelectric sensors and actuators are integrated continuously with the structural systems. In this manner, the piezoelectric sensor is able to detect the location and type of cracks that occur in the

* Corresponding author. Tel.: +98-21-600-5818; fax: +98-21-601-4828.
E-mail addresses: shodja@sina.sharif.ac.ir, shodja@sharif.edu (H.M. Shodja).

0020-7683/03/$ - see front matter © 2003 Elsevier Ltd. All rights reserved.
doi:10.1016/S0020-7683(03)00225-7

system. The piezoelectric devices experience stresses and deformation during their service life, therefore the need for reliability and optimum performance of such devices require investigations of their electromechanical behaviors.

Tiersten (1969) formulated the governing equations for the vibration of piezoelectric plates and investigated their fundamental electro-mechanical behavior. Two- and three-dimensional analysis of simply supported piezoelectric plates have been addressed by several investigators; see, for example, Ray et al. (1992), Heyliger and Brooks (1996), Ruan et al. (1999) for two-dimensional analysis, and Ray et al. (1993), Heyliger (1994), Bisegna and Maceri (1996), and Reddy and Cheng (2001) for three-dimensional analysis. In several of the above mentioned reports, some simplifications have been made. For example, Ray et al. (1993), presume that the three-three component of the piezoelectric tensor equal to zero, i.e. $e_{33} = 0$. As a result the continuities of normal electric induction field and electric potential at the interface between the layers are not satisfied. Ruan et al. (1999), have used an approximation for the distribution of electric potential through the thickness of the plate. Most of the reports in the literature are tailored for the treatments of simply supported rectangular piezoelectric plates. Henceforth, a unified approach which can accurately handle piezocomposite plates of arbitrary geometries consisting of layers with arbitrary thickness, and various types of boundary conditions is in order.

In the literature, most of the available exact closed-form solutions, are limited to simple geometries under simple applied loadings and boundary conditions. Whereas, the current investigation develops a general theory based on three-dimensional elasticity, without the need for any simplifying assumptions. The remarkable accuracy and robustness of the proposed approach are established by reconsideration of the problem examined by Heyliger (1994), a special case for which the exact closed-form solution exists. For demonstration of the generality and applicability of the present theory to complex irregular geometries, the solution to star-shaped piezocomposite plate is given. As another interesting application, the problem of perforated piezocomposite plate is addressed. The exact solutions for the star-shaped and the perforated plates mentioned above do not exist, moreover, due to the presence of sharp corners, interfaces, and irregularity in the geometry, its treatment by the existing numerical techniques such as finite element method would be a very difficult task.

2. Governing equations of piezoelectricity

The electromechanical behavior of piezoelectric materials is a coupled phenomenon. For linear piezoelectric medium, the stress $\boldsymbol{\sigma}$, strain $\mathbf{s}$, electric field $\mathbf{E}$, and electric induction $\mathbf{D}$ are related through the constitutive equations

$$\sigma_{ij} = C_{ijkl}s_{kl} - e_{kij}E_k, \quad i,j,k,l = 1,2,3, \tag{1a}$$

$$D_i = e_{ijk}s_{jk} + k_{ij}E_j, \quad i,j,k = 1,2,3. \tag{1b}$$

Employing the abridge notations $(ij) \to i$, and $(kl) \to j$ Eqs. (1a) and (1b) may equivalently be rewritten as

$$\sigma_i = C_{ij}s_j - e_{ki}E_k, \quad i,j = 1,2,\ldots,6 \text{ and } k = 1,2,3, \tag{2a}$$

$$D_i = e_{ik}s_k + k_{ij}E_j, \quad i,j = 1,2,3 \text{ and } k = 1,2,\ldots,6, \tag{2b}$$

where

$$\{\sigma_1 \quad \sigma_2 \quad \sigma_3 \quad \sigma_4 \quad \sigma_5 \quad \sigma_6\} \equiv \{\sigma_{11} \quad \sigma_{22} \quad \sigma_{33} \quad \sigma_{23} \quad \sigma_{13} \quad \sigma_{12}\}, \tag{3a}$$

$$\{s_1 \quad s_2 \quad s_3 \quad s_4 \quad s_5 \quad s_6\} \equiv \{s_{11} \quad s_{22} \quad s_{33} \quad 2s_{23} \quad 2s_{13} \quad 2s_{12}\}. \tag{3b}$$

The abridged components of the elastic moduli **C** in Eq. (2a) comply with the relations (3a) and (3b). **e** and **k** are the piezoelectric and dielectric tensors, respectively. For a displacement field **u** and electric potential function Φ we have

$$s_{ij} = \frac{1}{2}\left(\frac{\partial u_i}{\partial x_j} + \frac{\partial u_j}{\partial x_i}\right), \quad i,j = 1,2,3, \tag{4a}$$

$$E_i = -\frac{\partial \Phi}{\partial x_i}, \quad i = 1,2,3. \tag{4b}$$

In the SI system, the dimensions of the variables introduced above are as follows

$$\begin{aligned} &[\mathbf{s}] = [\ ], \quad [\boldsymbol{\sigma}] = \mathrm{N\,m^{-2}}, \quad [\mathbf{E}] = \mathrm{V\,m^{-1}} = \mathrm{N\,C^{-1}}, \\ &[\mathbf{D}] = \mathrm{C\,m^{-2}} = \mathrm{N\,V^{-1}\,m^{-1}}, \quad [\mathbf{C}] = \mathrm{N\,m^{-2}}, \\ &[\mathbf{e}] = \mathrm{N\,m^{-1}\,V^{-1}} = \mathrm{C\,m^{-2}}, \quad [\mathbf{k}] = \mathrm{C^2\,N^{-1}\,m^{-2}} = \mathrm{N\,V^{-2}}, \quad [\Phi] = V. \end{aligned} \tag{5}$$

In the absence of body forces and charges, the equilibrium equations and charge equation of electrostatics become

$$\sigma_{ij,j} = 0, \tag{6a}$$

$$D_{i,i} = 0. \tag{6b}$$

For convenience the following notations are introduced

$$P_{mn} = \begin{cases} C_{mn}, & 1 \leqslant m,n \leqslant 6, \\ e_{hm}, & 1 \leqslant m \leqslant 6, \quad 7 \leqslant n \leqslant 9, \\ e_{gn}, & 7 \leqslant m \leqslant 9, \quad 1 \leqslant n \leqslant 6, \\ -k_{gh}, & 7 \leqslant m \leqslant 9, \quad 7 \leqslant n \leqslant 9, \end{cases} \tag{7}$$

where P_{mn} is referred to as generalized modulus,

$$g = m - 6, \tag{8a}$$

$$h = n - 6. \tag{8b}$$

Similarly the generalized displacement U_m, generalized stress Σ_m, generalized strain S_m, and generalized traction T_m, are defined by

$$U_m = \begin{cases} u_m, & 1 \leqslant m \leqslant 3, \\ \Phi, & m = 4, \end{cases} \tag{9a}$$

$$\Sigma_m = \begin{cases} \sigma_m, & 1 \leqslant m \leqslant 6, \\ D_g, & 7 \leqslant m \leqslant 9, \end{cases} \tag{9b}$$

$$S_m = \begin{cases} s_m, & 1 \leqslant m \leqslant 6, \\ -E_g, & 7 \leqslant m \leqslant 9, \end{cases} \tag{9c}$$

$$T_m = \begin{cases} \sigma_{mj} n_j, & 1 \leqslant m \leqslant 3, \\ D_j n_j, & m = 4. \end{cases} \tag{9d}$$

In view of the above arguments, the generalized strain is written as

$$S_m = L_{mn} U_n, \tag{10}$$

where

$$\mathbf{L}^{\mathrm{T}} = \begin{bmatrix} \frac{\partial}{\partial x} & 0 & 0 & 0 & \frac{\partial}{\partial z} & \frac{\partial}{\partial y} & 0 & 0 & 0 \\ 0 & \frac{\partial}{\partial y} & 0 & \frac{\partial}{\partial z} & 0 & \frac{\partial}{\partial x} & 0 & 0 & 0 \\ 0 & 0 & \frac{\partial}{\partial z} & \frac{\partial}{\partial y} & \frac{\partial}{\partial x} & 0 & 0 & 0 & 0 \\ 0 & 0 & 0 & 0 & 0 & 0 & \frac{\partial}{\partial x} & \frac{\partial}{\partial y} & \frac{\partial}{\partial z} \end{bmatrix}. \tag{11}$$

Accordingly, Eqs. (2) and (6) are cast into the following generalized constitutive and generalized equilibrium equations

$$\Sigma_n = P_{mn} S_m, \tag{12}$$

$$L_{mn}\Sigma_m = 0, \quad m = 1,2,\ldots,9,\ n = 1,2,\ldots,4. \tag{13}$$

Combining Eqs. (10), (12) and (13) we obtain

$$A_{mn}U_n = 0, \tag{14}$$

where A_{mn} is the generalized equilibrium coefficient operator

$$A_{mn} = L_{im}P_{ij}L_{jn}. \tag{15}$$

The boundary conditions are expressed in the following manner

$$B_{mn}U_n = \begin{Bmatrix} T_m(U_n) - \overline{T}_m \\ U_m - \overline{U}_m \end{Bmatrix} = \mathbf{0}, \quad m,n = 1,2,\ldots,4, \tag{16}$$

in which B_{mn} is the generalized boundary condition operator, n_j is the direction cosine, and $\overline{T}_m$ is the prescribed generalized traction on the generalized traction boundary, Γ_Σ. $\overline{U}_m$ is the prescribed generalized displacement vector on the generalized displacement boundary, Γ_U.

The stored energy density W of a piezoelectric medium is given by:

$$W = \tfrac{1}{2}(S_i P_{ij} S_j), \tag{17}$$

which can be written as

$$W = \tfrac{1}{2}(\sigma_i s_i - E_k D_k) = \tfrac{1}{2}(C_{ij}s_i s_j - 2e_{kj}E_k s_j - k_{kl}E_k E_l), \quad i,j = 1,2,\ldots,6 \text{ and } k,l = 1,2,3. \tag{18}$$

The total energy functional, F of the system is

$$F = \int_\Omega W \,\mathrm{d}\Omega - \int_{\Gamma_\Sigma} T_m U_m \,\mathrm{d}\Gamma, \quad m = 1,2,\ldots,4. \tag{19}$$

Using the weighted residual Galerkin method and selecting δU_m as weight functions, the following variational relation holds

$$\delta F = 0. \tag{20}$$

3. A rational three-dimensional solution of the field equation

A versatile solution of Eq. (14) subjected to the boundary conditions (16) is sought. The proposed solution is obtained by the superposition of a special function which accommodates nonhomogeneous

kinematical boundary conditions and a series suitable for treating thick plates with arbitrary geometries. To this end the generalized displacement fields are expressed in the following form

$$U_m(x,y,z) = f_m(x,y,z) + \sum_{q=0}^{p}\sum_{l=0}^{q}\sum_{\alpha=0}^{q-l} C_{m\beta}\psi_{m\beta}(x,y,z), \quad m = 1,2,\ldots,4, \tag{21}$$

in which

$$\beta = \frac{q(q+1)(q+2)}{6} + \frac{(l+1)(2q-l+2)}{2} - \alpha. \tag{22}$$

The function $f_m(x,y,z)$ is such that the nonhomogeneous boundary conditions associated with the displacement field and electric potential are fulfilled. p is the order of polynomial, and $C_{m\beta}$ are the unknown coefficients. The functions $\psi_{m\beta}$, $m = 1,2,\ldots,4$ are taken as the product of general three-dimensional polynomials and functions, $\varphi_m^{(B)}(x,y,z)$ which enforce satisfaction of the kinematical boundary conditions and account for any symmetries present in the problem. Consideration of the symmetries leads to higher accuracies and substantial improvement in the convergence rate. The functions $\psi_{m\beta}(x,y,z)$ are defined by

$$\psi_{m\beta}(x,y,z) = x^{q-l-\alpha}y^{\alpha}z^{l}\varphi_m^{(B)}(x,y,z), \quad m = 1,2,\ldots,4, \tag{23}$$

with

$$\varphi_m^{(B)}(x,y,z) = \prod_{j=1}^{nb}[\Gamma_j^b(x,y,z)]^{\Omega_j^{bm}} \prod_{k=1}^{ns}[\Gamma_k^s(x,y,z)]^{\Omega_k^{sm}}, \quad m = 1,2,\ldots,4, \tag{24}$$

where ns is the number of plane of symmetries, Γ_k^s is the equation of the kth plane of symmetry, and

$$\Omega_k^{sm} = \begin{cases} 0, & \text{if } U_m \neq 0, \quad m = 1,2,\ldots,4, \quad \text{on the } k\text{th plane of symmetry,} \\ 1, & \text{if } U_m = 0, \quad m = 1,2,\ldots,4, \quad \text{on the } k\text{th plane of symmetry,} \end{cases} \tag{25}$$

nb is the number of boundaries, Γ_j^b is the equation of the jth boundary. For U_m, $m = 1,2,\ldots,4$, Ω_j^{bm} is defined by

$$\Omega_j^{bm} = \begin{cases} 0, & \text{if } U_m \neq 0 \text{ on the } j\text{th boundary,} \\ 1, & \text{if } U_m = 0 \text{ on the } j\text{th boundary.} \end{cases} \tag{26}$$

For smart multilayered piezoelectric composite plates consisting of k layers and associated generalized displacement field $U_m^k(x,y,z)$, some of the field variables are discontinuous across the interfaces. The discontinuities in the derivatives of the generalized displacement field are incorporated in the solution by letting

$$U_m^k(x,y,z) = f_m(x,y,z) + \sum_{q=0}^{p}\sum_{l=0}^{q}\sum_{\alpha=0}^{q-l} C_{m\beta}\psi_{m\beta}(x,y,z) + \sum_{q=0}^{p_k}\sum_{l=0}^{q}\sum_{\alpha=0}^{q-l} C_{m\beta}^k\psi_{m\beta}^k(x,y,z), \quad m = 1,2,\ldots,4, \tag{27}$$

where the first two terms in the right hand side of Eq. (27) have been introduced in Eq. (21). The third term consists of amending polynomials, $\psi_{m\beta}^k(x,y,z)$ of order P_k for layer k, with unknown coefficients $C_{m\beta}^k$. The amending polynomials are defined as

$$\psi_{m\beta}^k(x,y,z) = (x^{q-l-\alpha}y^{\alpha}z^{l})\varphi_m^{(B)k}(x,y,z), \quad m = 1,2,\ldots,4. \tag{28}$$

It should be emphasized that the values of the amending polynomials must be equal to zero at the interfaces,

$$\varphi_m^{(B)k}(x,y,z) = \varphi_m^{(B)}(x,y,z)\prod_{j=1}^{ni^k}[I_j^{\text{in}}(x,y,z)], \quad m = 1,2,\ldots,4, \tag{29}$$

where β and $\varphi_m^{(B)}$ are given by Eqs. (22) and (24) respectively, ni^k is the number of interfaces of the kth layer with other layers, and I_j^{in} is the equation of the surface of the jth associated interface. In this manner, the generalized displacement field remains continuous across the interfaces, while its derivatives can have the required discontinuities up to the desired orders. The unknown coefficients $C_{m\beta}$ are computed by minimization of the total energy functional

$$\frac{\partial F}{\partial C_{m\beta}} = 0. \tag{30}$$

4. Results and discussion

With the aid of the methodology developed in the previous section, three problems involving electromechanical loadings, homogeneous and nonhomogeneous boundary conditions are examined. The availability of the exact solution to the selected example of Section 4.1 provides a benchmark for establishment of the accuracy and robustness of the present analysis. As an interesting application of the current analysis to plates with arbitrary geometries, in Section 4.2 a star shape plate under mechanical loading is considered. For this example, the effects of the amending terms on the accuracy and convergence rate of the solutions are illuminated. In the last example given in Section 4.3, a piezoelectric rod with rectangular cross-section encased by a thick rectangular piezoelectric plate is solved under mechanical loading.

4.1. PZT—polymer composite plate

The piezoelectric composite plate considered here is a [0/90] cross-ply composed of an elastic layer in the middle and two piezoelectric layers which are bonded to its upper and lower surfaces, as shown in Fig. 1. The rectangular plate is simply supported along all its edges and has dimensions L_x, L_y and total thickness of H. The thickness of the elastic layer and the piezoelectric layers are $0.8H$ and $0.1H$, respectively. The material properties of the elastic and PZT-4 layers, which are both orthotropic materials, are given in Table 1. The origin of the coordinate system is set at the center of the plate, the z-axis is perpendicular to the layers and x and y axes are parallel to the main edges. The aspect ratio is assumed to be $L_x/H = L_y/H = 4.0$. Note that, for the present problem $H = 1$ m is used.

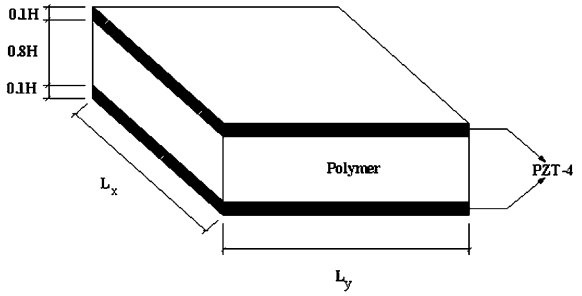

Fig. 1. Piezocomposite plate for the example given in Section 4.1.

Table 1
Electroelastic material properties

Property	PZT-4	$(Pb_{0.88}Ca_{0.12})(CO_{0.5}W_{0.5})_{0.04}Ti_{0.96}O_3$	Polymer
E1 (GPa)	81.3	127	132.38
E2	81.3	127	10.756
E3	64.5	119	10.756
ν_{23}	0.432	0.174	0.49
ν_{13}	0.432	0.174	0.24
ν_{12}	0.329	0.199	0.24
G_{23} (GPa)	25.6	53.5	3.606
G_{13}	25.6	53.5	5.654
G_{12}	30.6	53	5.654
e_{24} (C/m^2)	12.72	2.96	0
e_{15}	12.72	2.96	0
e_{31}	−5.2	0.8	0
e_{32}	−5.2	0.8	0
e_{33}	15.08	6.88	0
$\varepsilon_{11}/\varepsilon_0$	1475	202	3.5
$\varepsilon_{22}/\varepsilon_0$	1475	202	3
$\varepsilon_{33}/\varepsilon_0$	1300	181	3

4.1.1. Mechanical loading

In order to compare the results with the exact results reported in the literature, double sinusoidal loading on the upper surface with an amplitude equal to one is assumed

$$t_z = \cos\frac{\pi x}{L_x}\cos\frac{\pi y}{L_y}. \tag{31}$$

The sides, top and bottom surfaces are fixed at zero potential. Under these conditions, the basic functions are as follows:

$$\varphi_1^{(B)} = x(4y^2 - L_y^2), \tag{32}$$

$$\varphi_2^{(B)} = y(4x^2 - L_x^2), \tag{33}$$

$$\varphi_3^{(B)} = (4x^2 - L_x^2)(4y^2 - L_y^2), \tag{34}$$

$$\varphi_4^{(B)} = (4x^2 - L_x^2)(4y^2 - L_y^2)(4z^2 - H^2). \tag{35}$$

The following amending terms for the elastic layer are considered:

$$\varphi_m^{(B)\text{polymer}} = \varphi_m^{(B)}[z^2 - (0.4H)^2], \quad m = 1, 2, \ldots, 4. \tag{36}$$

For this example, the boundary conditions are homogeneous

$$f_m(x, y, z) = 0, \quad m = 1, 2, \ldots, 4, \tag{37}$$

where the values of these functions are equal to zero at the interfaces between the elastic and PZT-4 layers. These functions satisfy the continuity conditions for the displacement fields and the electric potential function. In solving this problem, amending terms have been incorporated. Variations of u, σ_x, σ_{xy}, and D_z with thickness are obtained by the proposed method and are plotted along with the exact solutions (Heyliger, 1994) in Figs. 2–5. Fig. 4 shows the discontinuity of shear stress σ_{xy} at the interface between layers. Fig. 5 confirms that, the electric induction D_z must be continuous at the interface. Comparison of

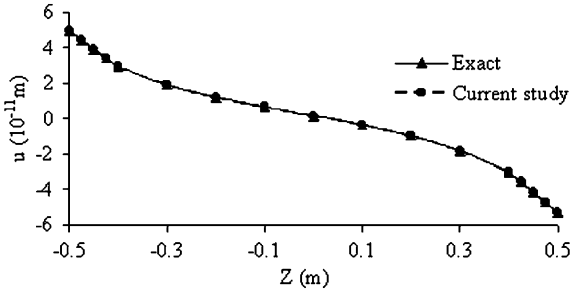

Fig. 2. Distribution of the in plane displacement u along the z-axis, pertinent to the example of Section 4.1.1.

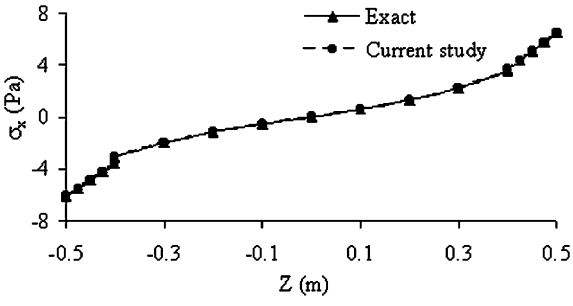

Fig. 3. Distribution of the normal stress σ_x along the z-axis, pertinent to the example of Section 4.1.1.

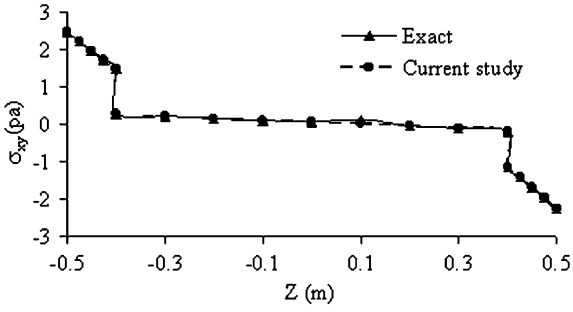

Fig. 4. Distribution of shear stress σ_{xy} along the z-axis, pertinent to the example of Section 4.1.1.

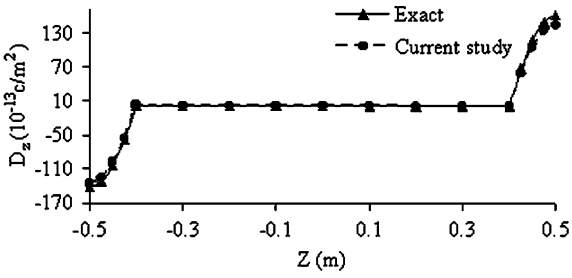

Fig. 5. Distribution of the electric induction D_z along the z-axis, pertinent to the example of Section 4.1.1.

Table 2
In plane displacement, electric potential and normal stress in z-direction obtained for different points along the thickness of the plate, pertinent to the example of Section 4.1.1

Z (m)	u (10^{-11} m)		Φ (10^{-3} V)		σ_z (Pa)	
	Exact	Current study	Exact	Current study	Exact	Current study
−0.5	4.9666	4.9663	0	0	0	0.0019
−0.475	4.4401	4.4397	2.224	2.1399	0.0034	0.002
−0.45	3.9246	3.9242	4.25	4.0523	0.0131	0.0127
−0.425	3.419	3.4187	6.02	5.7388	0.0284	0.023
−0.4	2.9218	2.9215	7.56	7.2028	0.0486	0.0537
−0.4	2.9218	2.9215	7.56	7.2028	0.0486	0.0084
−0.3	1.9141	1.9139	7.06	6.6754	0.1482	0.1326
−0.2	1.196	1.196	6.65	6.2373	0.2613	0.2625
−0.1	0.644	0.6443	6.34	5.8827	0.3804	0.3692
0	0.16	0.1603	6.11	5.6068	0.4983	0.5142
0.1	−0.346	−0.3463	5.96	5.4059	0.6168	0.623
0.2	−0.968	−0.968	5.89	5.2773	0.7374	0.7606
0.3	−1.816	−1.8156	5.89	5.2193	0.8519	0.8539
0.4	−3.0336	−3.0334	5.98	5.2311	0.9515	0.9171
0.4	−3.0336	−3.0334	5.98	5.2311	0.9515	0.9628
0.425	−3.5918	−3.5916	4.88	4.3028	0.9715	0.9713
0.45	−4.1593	−4.1589	3.58	3.1228	0.9868	0.9882
0.475	−4.7375	−4.7371	1.89	1.6897	0.9965	0.996
0.5	−5.3277	−5.3274	0	0	1	1.0018

Table 3
Electric induction, normal and shear stresses obtained for different points along the thickness of the plate, pertinent to the example of Section 4.1.1

Z (m)	D_z (10^{-13} C/m^2)		σ_x (Pa)		σ_{xy} (Pa)	
	Exact	Current study	Exact	Current study	Exact	Current study
−0.5	−142.46	−136.2228	−6.1498	−6.1483	2.4682	2.4678
−0.475	−132.4	−126.2617	−5.5096	−5.5098	2.2151	2.2151
−0.45	−103.66	−98.3297	−4.8781	−4.8776	1.9675	1.9671
−0.425	−58.352	−56.0148	−4.254	−4.2556	1.7246	1.7243
−0.4	1.4587	2.7818	−3.6366	−3.6327	1.4859	1.4857
−0.4	1.4587	1.5251	−3.1019	−3.1152	0.2745	0.2745
−0.3	1.1995	1.2792	−2.0028	−2.0062	0.204	0.204
−0.2	0.9563	1.0503	−1.2018	−1.1991	0.1494	0.1494
−0.1	0.7259	0.8354	−0.5718	−0.5747	0.1033	0.1033
0	0.5052	0.6317	−0.0102	−0.0068	0.0597	0.0597
0.1	0.2913	0.4364	0.5756	0.5726	0.0129	0.0129
0.2	0.0813	0.2471	1.2819	1.2845	−0.0431	−0.0431
0.3	−0.1276	0.0609	2.223	2.2192	−0.1151	−0.1151
0.4	−0.3382	−0.1244	3.5478	3.5335	−0.2117	−0.2117
0.4	−0.3382	−0.9048	3.6746	3.6794	−1.1458	−1.1456
0.425	66.568	57.8324	4.3677	4.3671	−1.4151	−1.4148
0.45	117.23	104.3737	5.0678	5.0691	−1.6886	−1.6883
0.475	149.35	133.2258	5.7762	5.7767	−1.9669	−1.9669
0.5	160.58	143.1816	6.4938	6.4955	−2.2508	−2.2504

other results obtained by the present method with the exact solutions are displayed in Tables 2 and 3. This problem is analyzed using ninth degree polynomials. The convergence rates for the displacement w and the

Table 4
Convergence rate for the vertical displacement and electric induction, pertinent to the example of Section 4.1.1

Order of polynomials	$w\ (x=0,y=0,z=H/2)$ (10^{-11} m)	$D_z\ (x=0,y=0,Z=H/2)$ (10^{-13} C/m^2)
0	8.5535	−776.359
1	16.4294	−19971.359
2	18.2283	−1970.088
3	29.014	−351.38
4	29.0899	−179.1163
5	30.2991	−205.361
6	30.3167	−201.692
7	30.3922	−133.497
8	30.3922	−133.79
9	30.3951	−136.221
Exact solution	30.3962	−142.46

electric induction D_z at point $(0,0,H/2)$ are shown in Table 4. It is inferred that, the value of w converges to the exact solutions faster than that of D_z, which is a function of derivatives of displacements and electric potential. Therefore, one may conclude that, the values of displacements and electric potential converge to the exact solutions faster than those for quantities like stresses and electric induction, which depend on the derivatives of displacement and electric potential.

4.1.2. Electrical loading

For the sake of comparisons of the results with the exact results reported in literature, double sinusoidal potential on the upper surface with an amplitude equal to one, and zero potential on the lower surface are assumed. The electric loading is given by

$$\Phi = \cos\frac{\pi x}{L_x}\cos\frac{\pi y}{L_y} \quad \text{at } z=\frac{H}{2}, \tag{38}$$

and

$$\Phi = 0 \quad \text{at } z=\frac{-H}{2}. \tag{39}$$

For this problem the boundary functions and the boundary functions associated with the amending terms are the same as the ones given in the previous example. The nonhomogeneous boundary condition dictates $f_m(x,y,z)$ to be defined as follows

$$\begin{aligned} &f_m(x,y,z)=0, \quad m=1,2,3,\\ &f_4(x,y,z)=\left(\frac{1}{2}+\frac{z}{H}\right)\cos\frac{\pi x}{L_x}\cos\frac{\pi y}{L_y}. \end{aligned} \tag{40}$$

In this example ninth degree amending terms and general polynomials are considered. Results showing the variations of: electric potential Φ; normal stress σ_x; shear stresses σ_{xy} and σ_{xz}; and electric induction D_z, with thickness along with the exact solutions (Heyliger, 1994) are plotted in Figs. 6–10. The results for other quantities are compared with the exact solutions in Tables 5 and 6.

4.2. A star shape plate consisting of two piezoceramic layers

To demonstrate the applicability of the proposed analysis to plates of irregular shapes, the star shape piezocomposite system under nonuniform loading is considered, Fig. 11. The equation of the boundary of the plate in the polar coordinate system (r,θ) is

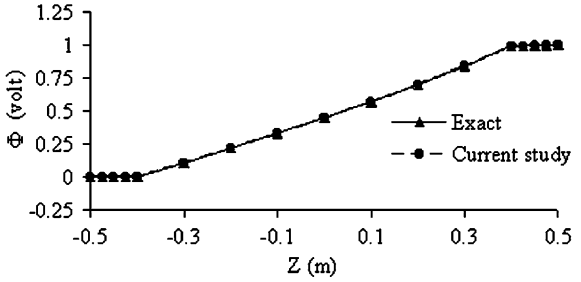

Fig. 6. Distribution of the electric potential along the z-axis, pertinent to the example of Section 4.1.2.

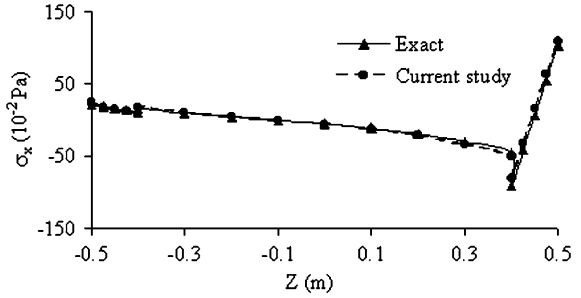

Fig. 7. Distribution of the normal stress σ_x along the z-axis, pertinent to the example of Section 4.1.2.

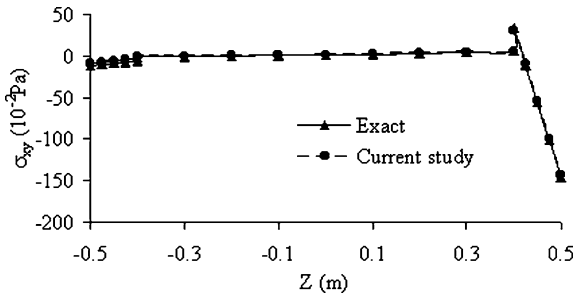

Fig. 8. Distribution of the shear stress σ_{xy} along the z-axis, pertinent to the example of Section 4.1.2.

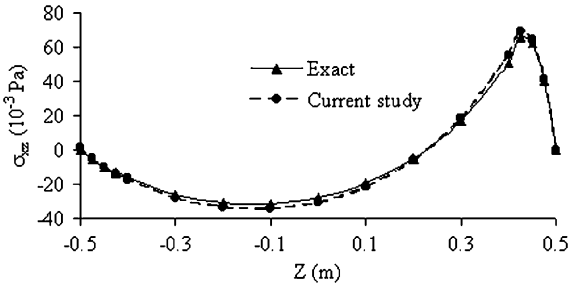

Fig. 9. Distribution of the shear stress σ_{xz} along the z-axis, pertinent to the example of Section 4.1.2.

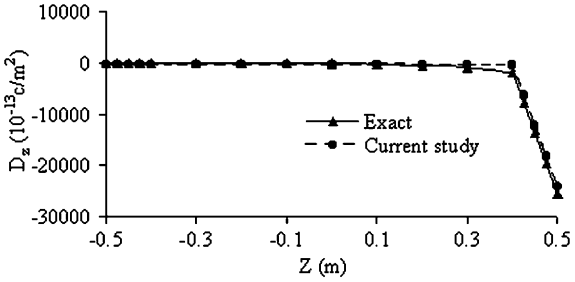

Fig. 10. Distribution of the electric induction D_z along the z-axis, pertinent to the example of Section 4.1.2.

Table 5
Electric potential and displacements obtained for different points along the thickness of the plate, pertinent to the example of Section 4.1.2

Z (m)	Φ (V)		w (10^{-12} m)		u (10^{-12} m)	
	Exact	Current study	Exact	Current study	Exact	Current study
−0.5	0	0	−13.31	−13.654	−2.463	−2.786
−0.475	−0.0004	−0.00003	−13.337	−13.695	−2.222	−2.519
−0.45	−0.0008	−0.00003	−13.36	−13.733	−1.985	−2.257
−0.425	−0.0009	−0.00002	−13.377	−13.759	−1.751	−1.999
−0.4	−0.001	0.00001	−13.39	−13.78	−1.52	−1.743
−0.4	−0.001	0.00001	−13.39	−13.78	−1.52	−1.743
−0.3	0.1081	0.10829	−13.402	−13.797	−0.923	−1.062
−0.2	0.2179	0.21802	−13.385	−13.761	−0.454	−0.53
−0.1	0.3305	0.33066	−13.343	−13.732	−0.034	−0.055
0	0.4476	0.44773	−13.271	−13.663	0.409	0.439
0.1	0.5705	0.57077	−13.158	−13.534	0.949	1.036
0.2	0.7014	0.70146	−12.987	−13.375	1.676	1.838
0.3	0.8415	0.84155	−12.729	−13.12	2.707	2.977
0.4	0.9929	0.99289	−12.346	−12.723	4.205	4.626
0.4	0.9929	0.99289	−12.346	−12.723	4.205	4.626
0.425	0.9936	0.99363	−12.431	−12.756	−5.193	−4.752
0.45	0.995	0.99507	−12.868	−13.115	−14.593	−14.132
0.475	0.9971	0.99719	−13.658	−13.801	−24.014	−23.533
0.5	1	1	−14.802	−14.821	−33.474	−32.974

$$r(1 + 0.1\cos 6\theta) - 3 = 0. \tag{41}$$

The plate consists of two piezoceramic layers of equal thicknesses, namely PZT-4 and $(Pb_{0.88}Ca_{0.12})((Co_{0.5}W_{0.5})_{0.04}Ti_{0.96})O_3$ whose material properties are displayed in Table 1. The origin of the coordinate system is set at the centroid of the plate. The plate is simply supported and has a total thickness of $H = 1$ m.

4.2.1. Mechanical loading

Suppose that the applied mechanical loading on the upper face of the plate is of the form

$$t_z = \sin\frac{\pi}{6}[3 - r(1 + 0.1\cos 6\theta)], \quad \text{on } z = \frac{H}{2}. \tag{42}$$

Let u, v, and w be the displacements in the x-, y-, and z-directions, respectively. For this problem, the appropriate boundary functions corresponding to the displacements u, v, w, and electric potential function Φ are

Table 6
Stresses and electric induction obtained for different points along the thickness of the plate, pertinent to the example of Section 4.1.2

Z (m)	σ_x (10^{-2} Pa)		σ_{xy} (10^{-2} Pa)		σ_{xz} (10^{-2} Pa)		D_z (10^{-13} C/m^2)	
	Exact	Current study	Exact	Current study	Exact	Current study	Exact	Current study
−0.5	21.998	24.153	−11.276	−8.622	0	1.218	−9.7	−255.1
−0.475	19.072	18.46	−9.944	−7.244	−5.245	−4.72	−9.9	−280.7
−0.45	16.173	15.119	−8.635	−5.726	−9.693	−10.057	−10.7	−300.1
−0.425	13.295	12.005	−7.346	−4.232	−13.349	−13.804	−11.7	−312.4
−0.4	10.435	8.433	−6.073	−2.861	−16.219	−17.025	−13.1	−322.6
−0.4	15.713	18.175	−1.122	−0.526	−16.219	−16.701	−13.1	−286.9
−0.3	9.243	10.732	−0.584	0.128	−25.983	−27.945	−16.3	−288.9
−0.2	4.082	4.962	−0.057	0.727	−30.786	−33.35	−28.1	−294.7
−0.1	−0.581	−0.551	0.523	1.426	−31.346	−34.29	−54.6	−304.4
0	−5.482	−5.919	1.229	2.001	−27.741	−30.676	−109.8	−318.2
0.1	−11.397	−12.345	2.21	2.856	−19.429	−21.633	−222.6	−336.2
0.2	−19.249	−21.261	3.325	3.615	−5.167	−5.914	−452.2	−358.8
0.3	−30.247	−33.263	4.663	5.134	17.163	18.607	−919.2	−386.2
0.4	−46.061	−50.754	6.337	5.646	50.86	55.71	−1868.6	−418.7
0.4	−90.305	−81.047	34.295	30.588	50.86	55.754	−1868.6	−431.3
0.425	−41.864	−32.384	−10.698	−8.636	65.738	69.359	−7788.2	−6355.1
0.45	6.538	15.927	−55.693	−53.681	62.233	64.59	−13714	−12283.3
0.475	55	64.126	−100.77	−99.077	40.337	41.44	−19654	−18203.2
0.5	103.622	108.898	−146.03	−143.082	0	−0.515	−25616	−24173.9

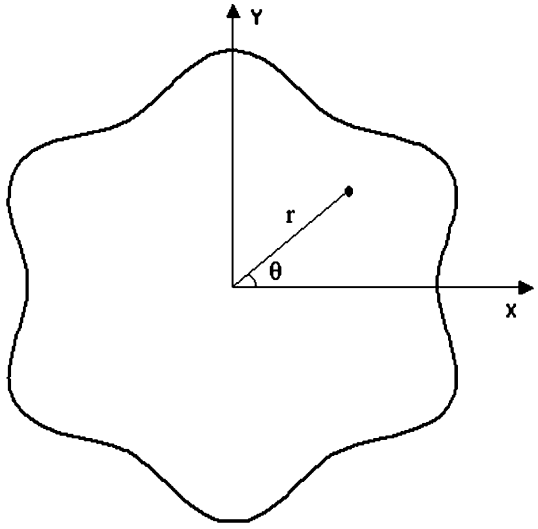

Fig. 11. Star shape piezocomposite plate for the example given in Section 4.2.

$$\varphi_1^{(B)} = x, \tag{43}$$

$$\varphi_2^{(B)} = y, \tag{44}$$

$$\varphi_3^{(B)} = [r(1 + 0.1\cos 6\theta)]^2 - 9, \tag{45}$$

$$\varphi_4^{(B)} = (4z^2 - H^2)\{[r(1 + 0.1\cos 6\theta)]^2 - 9\}, \tag{46}$$

respectively. For this problem the kinematical boundary conditions are homogeneous

$$f_m(x, y, z) = 0, \quad m = 1, 2, \ldots, 4. \tag{47}$$

Incorporation of the discontinuities in the derivatives of displacement fields and electric potential function through the amending terms results in considerable improvement of the accuracy and convergence rate. The amending terms associated with the layer made up of PZT-4 may be written as

$$\varphi_m^{(B)\text{PZT-4}} = \varphi_m^{(B)} z, \quad m = 1, 2, \ldots, 4, \tag{48}$$

where the superscript PZT-4 corresponds to the material properties of the layer. To establish the effects of the amending terms, the results on the variations of: electric potential Φ; shear stress σ_{xz}; and electric induction D_z through the thickness of the plate are computed with and without the amending terms and the results are compared, Figs. 12–14. In Fig. 13, the value of σ_{xz} is being plotted through the thickness at point A ($x = -2.7, y = 0$), whereas the values of D_z and Φ shown in Figs. 12 and 14, respectively correspond to the center of the plate. The variation of the displacement w on $y = 0$ and $z = H/2$, along the x-direction is shown in Fig. 15. It is seen that, while the effects of the amending terms on the electric potential and on the vertical displacement are negligible, their influences on the stress σ_{xz} and the electric induction D_z are great. When the amending terms are included, the continuities of σ_{xz} and D_z at the interface, $z = 0$ are correctly computed. Exclusion of the amending terms yielded dramatic discontinuities at the interface, $z = 0$. Although consideration of the amending terms has very little effects on the displacement field and the

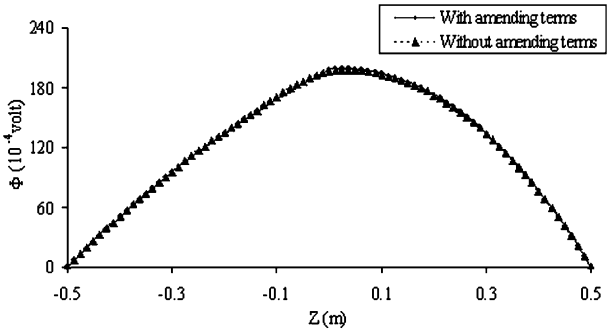

Fig. 12. Distribution of the electric potential through the thickness at the center of the plate, pertinent to the example of Section 4.2.1.

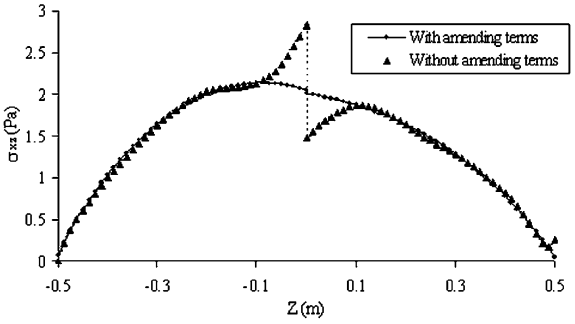

Fig. 13. Distribution of the shear stress σ_{xz} through the thickness at point A, pertinent to the example of Section 4.2.1.

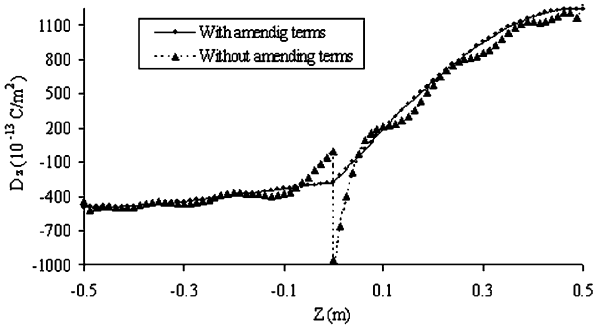

Fig. 14. Distribution of the electric induction D_z through the thickness at the center of the plate, pertinent to the example of Section 4.2.1.

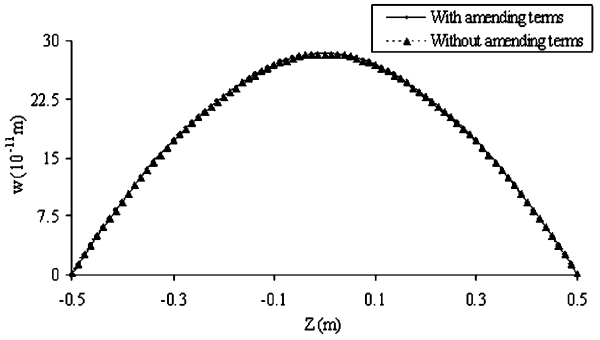

Fig. 15. Distribution of the displacement w along the x-axis at $y = 0$ and $z = H/2$, pertinent to the example of Section 4.2.1.

electric potential, but their roles in computations of quantities like stress fields and electric induction, which depend on the derivatives of the displacements and electric potential are quite important. Fig. 16 displays the variation of the displacement u through the thickness of the plate at point A. The distributions of the displacement w, normal stresses σ_x and σ_z corresponding to the center of the plate are shown in Figs. 17–19, respectively. Note that, σ_z attains, with high precision, the values of 0 and 1 on the lower and upper surface

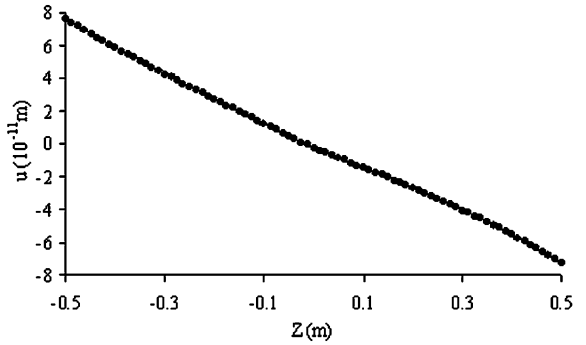

Fig. 16. Distribution of the in plane displacement u through the thickness at point A, pertinent to the example of Section 4.2.1.

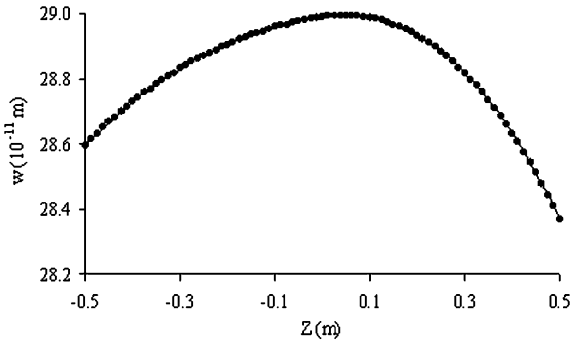

Fig. 17. Distribution of the displacement w through the thickness at the center of the plate, pertinent to the example of Section 4.2.1.

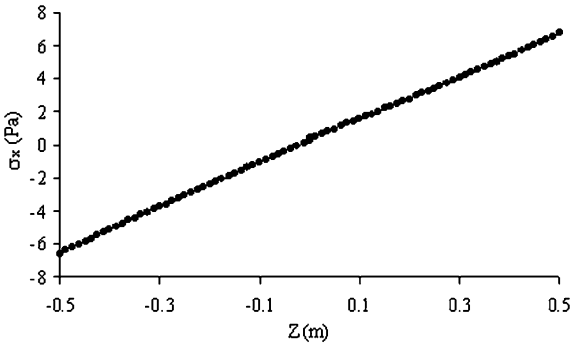

Fig. 18. Distribution of the normal stress σ_x through the thickness at the center of the plate, pertinent to the example of Section 4.2.1.

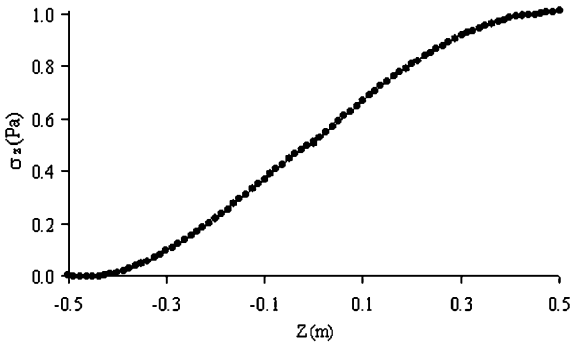

Fig. 19. Distribution of the normal stress σ_z through the thickness at the center of the plate, pertinent to the example of Section 4.2.1.

of the plate, respectively. Moreover, the continuity of σ_z at the interface between the two layers is accurately captured. In this subsection the calculations are carried out using 15th degree polynomials.

4.3. Perforated piezocomposite plate

As an interesting example, consider the piezocomposite system shown in Fig. 20, where a piezoelectric rod of rectangular cross-section is placed into a perforated thick plate whose piezoelectric properties are

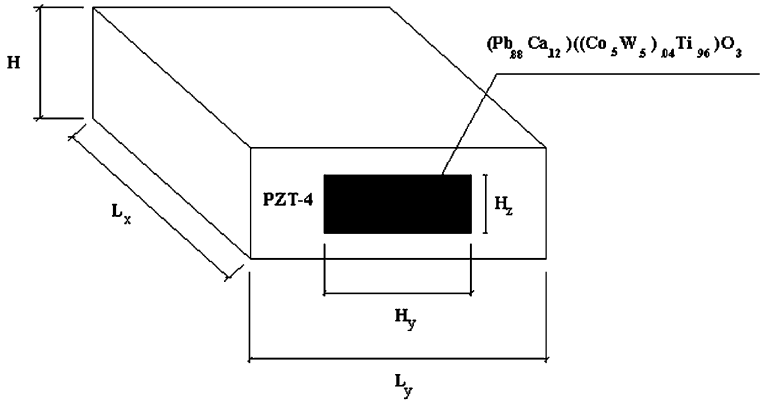

Fig. 20. Perforated piezocomposite plate for the example given in Section 4.3.

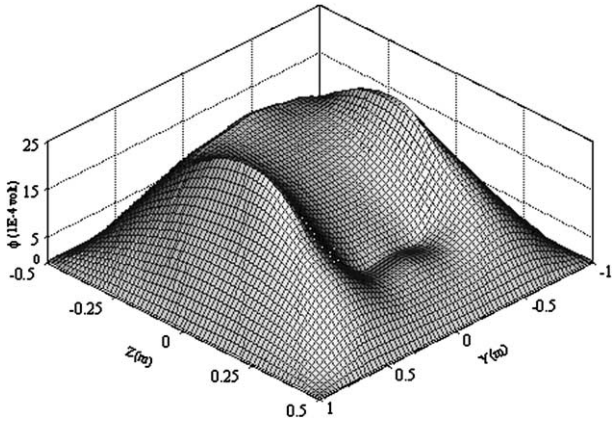

Fig. 21. Distribution of the electric potential in the y–z plane, for the example of Section 4.3.1.

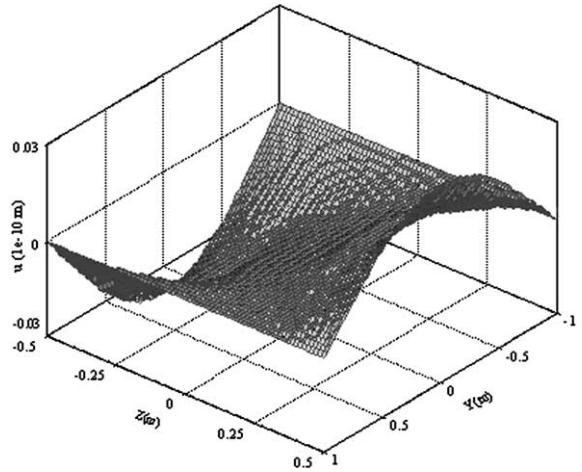

Fig. 22. Distribution of the displacement in x-direction in the y–z plane, for the example of Section 4.3.1.

different from those for the rod. The material properties for each domain are given in Table 1. The dimensions of the plate are $H = 1$ m, $L_x = L_y = 2$ m and the dimensions of the rod are $H_x = 2$ m, $H_y = 1$ m, $H_z = 0.5$ m. The plate is simply supported. The origin of the Cartesian coordinates is located at the centroid of the piezocomposite system.

4.3.1. Mechanical loading

The upper face of the piezocomposite system is subjected to the following normal traction

$$t_z = \cos\frac{\pi x}{L_x}\cos\frac{\pi y}{L_y}. \tag{49}$$

The electric potential on all faces are set equal to zero. For the example considered in this section, the displacement and the electric potential boundary functions are the same as the ones presented for the example studied in Section 4.1. In view of having homogeneous boundary conditions,

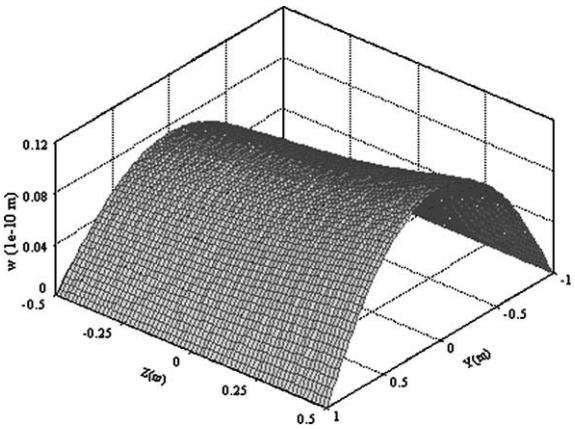

Fig. 23. Distribution of the displacement in z-direction in the y–z plane, for the example of Section 4.3.1.

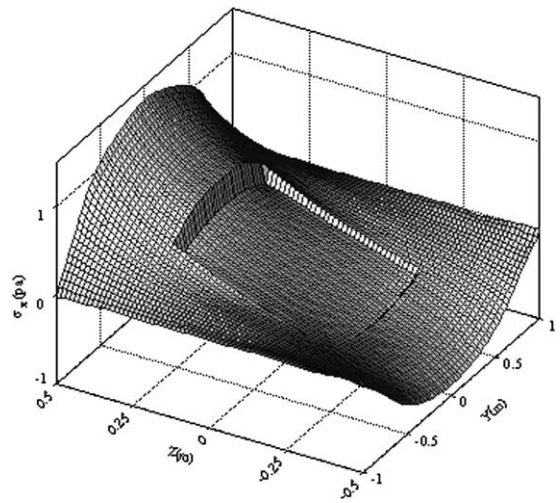

Fig. 24. Distribution of the normal stress σ_x in the y–z plane, for the example of Section 4.3.1.

$$f_m(x,y,z) = 0, \quad m = 1,2,\ldots,4, \tag{50}$$

and the boundary functions for the rod may be written as

$$\varphi_m^{(B)\mathrm{rod}} = \varphi_m^{(B)} \lfloor (4y^2 - H_y^2)(4z^2 - H_z^2) \rfloor, \quad m = 1,2,3,4. \tag{51}$$

Fifteenth degree amending terms and general polynomials for the displacements and electric potential are employed. Figs. 21–30 show the distribution of: electric potential Φ; displacements u and w; stresses σ_x, σ_y, σ_z, σ_{xy}, σ_{xz}, σ_{yz}; and electric induction D_z in the y–z plane. It is observed that the presence of the piezoelectric rod of rectangular cross-section remarkably disturbs the electromechanical field.

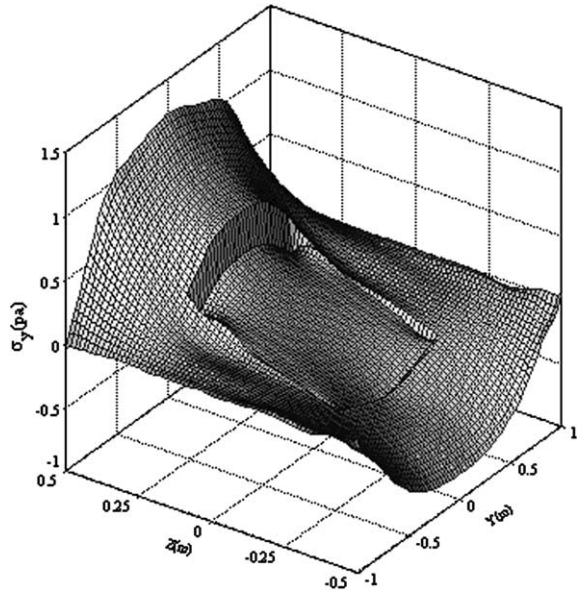

Fig. 25. Distribution of the normal stress σ_y in the y–z plane, for the example of Section 4.3.1.

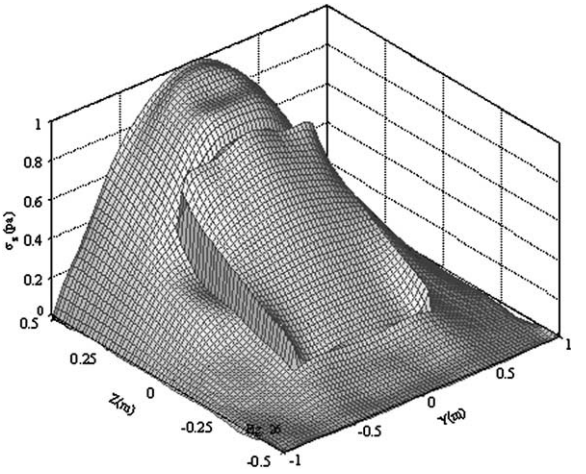

Fig. 26. Distribution of the normal stress σ_z in the y–z plane, for the example of Section 4.3.1.

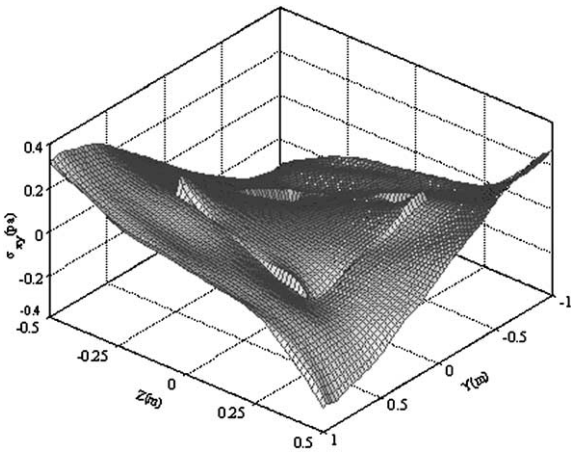

Fig. 27. Distribution of the shear stress σ_{xy} in the y–z plane, for the example of Section 4.3.1.

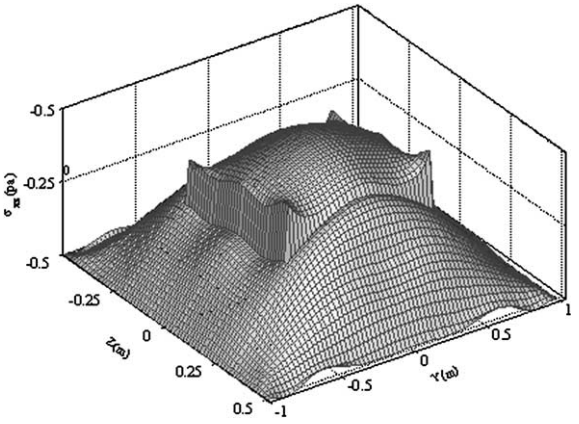

Fig. 28. Distribution of the shear stress σ_{xz} in the y–z plane, for the example of Section 4.3.1.

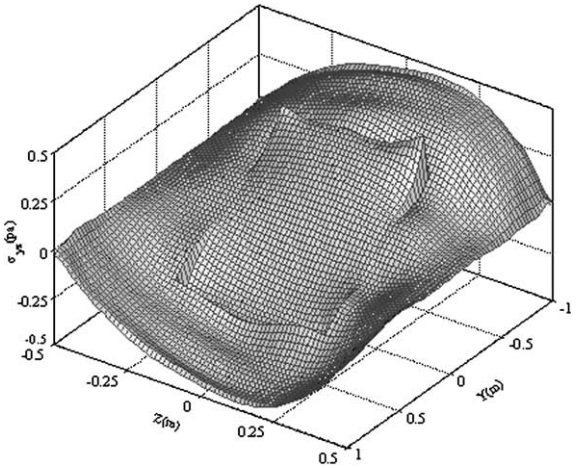

Fig. 29. Distribution of the shear stress σ_{yz} in the y–z plane, for the example of Section 4.3.1.

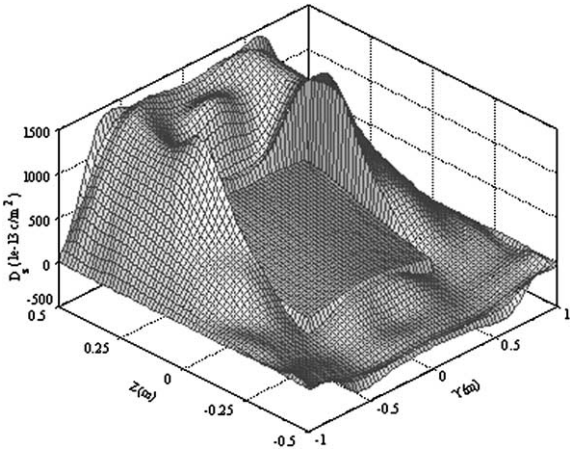

Fig. 30. Distribution of the electric induction D_z in the y–z plane, for the example of Section 4.3.1.

5. Conclusion

A rational three-dimensional treatment of piezocomposite plates with arbitrary geometry and boundary conditions subjected to electromechanical loadings is given. Continuity of the generalized displacements and tractions across the interfaces are enforced through introduction of the amending terms. If the derivatives of the generalized displacements are discontinuous across any interface, it is seen that exclusion of the amending terms for the associated quantities may lead to unrealistic results at that interface. Incorporation of the amending terms has a remarkable role in improvement of the accuracy and convergence rate. Another key feature of the proposed method is the relative ease in modeling nonhomogeneous kinematical boundary conditions, such as applying electric potential. In addition to the multilayer piezocomposites, the present method can easily handle piezocomposites containing inhomogeneities of various geometries.

Acknowledgement

This work was in part supported by Sharif University of Technology.

References

Bisegna, P., Maceri, F., 1996. An exact three-dimensional solution for simply supported rectangular piezoelectric plates. ASME Journal of Applied Mechanics 63, 628–638.

Forward, R.L., 1979. Electronic sampling of vibration in optical structures. Applied Optics, 690–697.

Heyliger, P., 1994. Static behavior of laminated elastic/piezoelectric plates. AIAA Journal 32 (12), 2481–2488.

Heyliger, P., Brooks, S., 1996. Exact solutions for laminated piezoelectric plates in cylindrical bending. ASME Journal of Applied Mechanics 63, 903–910.

Ray, M.C., Bhattacharya, R., Samanta, B., 1993. Exact solution for static analysis of intelligent structures. AIAA Journal 31, 1684–1691.

Ray, M.C., Rao, K.M., Samanta, B., 1992. Exact analysis of coupled electrostatic behavior of a piezoelectric plate under cylindrical bending. Computers and Structures 45, 667–677.

Reddy, J.N., Cheng, Z.Q., 2001. Three-dimensional solutions of smart functionally graded plates. ASME Journal of Applied Mechanics 68, 234–241.

Ruan, X., Danforth, S.C., Safari, A., Chou, T.W., 1999. A theoretical study of the coupling effects in piezoelectric ceramics. International Journal of Solids and Structures 36, 465–487.

Tiersten, H.F., 1969. Linear Piezoelectric Plate Vibration. Plenum, New York (Chapter 5).